Channel Estimation for Doubly-Spread Channels

Stefano Mangione
stefano.mangione.tlc@unipa.it
Università degli Studi di Palermo
Palermo, Italy

Giovanni Garbo
giovanni.garbo@unipa.it
Università degli Studi di Palermo
Palermo, Italy

Abstract

This paper presents a novel method for low-complexity estimation of doubly spread channels, specifically channels with path-dependent Doppler scaling. A time selectivity phenomenon, specifically appearing on doubly spread channels, and impairing methods based on autocorrelation, is described. To devise a low complexity method, we propose employing a composite preamble made of hyperbolic chirps, and a greedy path-matching algorithm at the receiver. The performance of the method is evaluated through simulations, and we show its effectiveness in shallow water scenarios. The advantage in computational complexity with respect to state-of-the-art methods like orthogonal matching pursuit is discussed.

CCS Concepts

• **Hardware → Signal processing systems**; **Sensor devices and platforms**; **Sound-based input / output**; **Wireless devices**.

Keywords

Channel estimation, Doubly spread channels

ACM Reference Format:
Stefano Mangione and Giovanni Garbo. 2025. Channel Estimation for Doubly-Spread Channels. In *The 19th International Conference on Underwater Networks and Systems (WUWNet '25), October 29–31, 2025, Shenzhen, China.* ACM, New York, NY, USA, 8 pages. https://doi.org/10.1145/3784941.3784959

1 Introduction

Underwater acoustic (UWA) communication systems face unique challenges due to the propagation characteristics of the underwater channel. With respect to radio frequency communications, the principal issue faced by UWA communication systems is the strong Doppler effect caused by the low speed of sound and the mobility of transmitters, receivers, and the medium itself [14].

In particular, any mobility in presence of multipath propagation with a significant angle spread (at the transmitter or at the receiver) results in a received signal made of delayed and time-scaled replicas, with interference anytime the time-varying propagation delays are comparable.

Several Doppler estimation methods in the literature assume that the received signal is affected by a common scaling factor [4, 7–9, 11, 17, 19–21]. This hypothesis holds when there is a dominant path so that the superposed rescaled signals appear as a negligible interference, or the propagation delays result sparse so that the reception events are independent. This may happen in deep ocean when the transmitter and receiver are sufficiently far from the acoustic impedance interfaces.

In the shallow water scenario, or when the transmitter and or receiver are close to the surface, the doubly-spread nature of the channel cannot be neglected, and in order to use receiver structures with coherent detection (e.g. [18]), some method must be used in order to estimate the channel, such as methods based on orthogonal matching pursuit (OMP) [3, 6, 15], or other signal space-based methods [5, 22]. The fallback modulation used in this case is usually a robust modulation with non-coherent detection, such as frequency-hopping binary FSK [12].

In this paper, we propose a low complexity method based on the properties of hyperbolic frequency modulated signals [1], starting from [8, 20] and extending it to counter a time-aliasing phenomenon we observed.

The main contributions of this work are:

- a simplified channel model for path-dependent Doppler scaling
- present the time-aliasing phenomenon that can manifest itself in the received signal, and why autocorrelation-based methods will fail
- devise a counter strategy based on the rationale behind the time-aliasing phenomenon, and show how the proposed method is superior to other low-complexity methods

The remainder of this paper is organized as follows. Section 2 presents a simplified model for path-dependent Doppler scaling. Section 3 reviews channel estimation approaches and identifies their limitations. Section 4 recalls the properties of hyperbolic frequency modulated signals, their detection and a method for joint delay and Doppler estimation generalizing [8, 20]. Section 5 presents the time-aliasing issue featured by doubly-spread channels, and presents our proposed greedy estimation method. Section 6 provides simulation results and performance analysis. Section 7 concludes the paper.

2 Linear Time-Varying Channels

We denote by $y(t) = S\{x(t_x); t\}$ the input-output relationship of a general system, where t_x and t denote respectively the time variables of the input and output signals.

We consider a linear time-varying (LTV) [2] channel whose impulse response is defined as:

$$h(t; t_\delta) = S\{\delta(t_x - t_\delta); t + t_\delta\} \tag{1}$$

where t_δ is the instant at which the Dirac delta is applied to the system.

Note that in (1) the impulse response is shifted towards the time origin, so that $h(t; t_\delta)$ is always zero for $t < 0$ for a causal system. This definition differs from the usual definition in the literature [2],

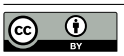

WUWNet '25, Shenzhen, China

ACM ISBN 979-8-4007-2316-2/2025/10
https://doi.org/10.1145/3784941.3784959

but it is preferred here, as we find it more intuitive, and degenerates to the usual impulse response in the time-invariant case.

With the previous definition, the noiseless LTV channel output is

$$y(t) = S\{x(t_x); t\} = \int x(t_\delta) h(t - t_\delta; t_\delta) dt_\delta \tag{2}$$

which clearly turns into a convolution product when the system is time-invariant.

With the assumption that the channel can be described by the multipath propagation model, we have:

$$h(t; t_\delta) = \sum_{l=1}^{L} \rho_l(t_\delta) \delta(t - \tau_l(t_\delta)) \tag{3}$$

where $\rho_l(t)$ and $\tau_l(t)$ are the time-varying path amplitudes and delays, as functions of the time at which the Dirac is presented *at the input* of the channel.

Substituting (3) in (2), we obtain:

$$y(t) = \sum_{l=1}^{L} \int x(t_\delta) \rho_l(t_\delta) \delta(t - t_\delta - \tau_l(t_\delta)) dt_\delta. \tag{4}$$

With the substitution $\xi = \xi_l(t_\delta) = t_\delta + \tau_l(t_\delta) \implies t_\delta = \xi_l^{-1}(\xi)$, we obtain:

$$y(t) = \sum_{l=1}^{L} \int x(\xi_l^{-1}(\xi)) \rho_l(\xi_l^{-1}(\xi)) \delta(t - \xi) \frac{1}{|\xi_l'(\xi)|} d\xi, \tag{5}$$

which, by virtue of the Dirac sampling property, results:

$$y(t) = \sum_{l=1}^{L} \frac{1}{|\xi_l'(t)|} \rho_l(\xi_l^{-1}(t)) x(\xi_l^{-1}(t)). \tag{6}$$

2.1 Single propagation path

To exemplify the previous argument, let us consider a single-path ($L = 1$) mono-dimensional channel, where the transmitter and receiver positions are respectively described by the laws

$$p_{\text{tx}}(t) = v_{\text{tx}} t \tag{7}$$

$$p_{\text{rx}}(t) = d + v_{\text{rx}} t \tag{8}$$

and where we assume, without loss of generality, that $p_{\text{tx}}(0) = 0$ and $p_{\text{rx}}(t_\delta) \geq p_{\text{tx}}(t_\delta)$. With the further assumption, for simplicity, of a constant sound propagation speed c, the propagation delay $\tau(t_\delta)$ for an impulse entering the channel at t_δ is obtained by solving the equation:

$$p_{\text{rx}}(t_\delta + \tau) = p_{\text{tx}}(t_\delta) + c\tau. \tag{9}$$

It is straightforward to find

$$\tau(t_\delta) = \frac{d + (v_{\text{rx}} - v_{\text{tx}}) t_\delta}{c - v_{\text{rx}}}. \tag{10}$$

In turn,

$$\xi = \xi(t_\delta) = t_\delta + \tau(t_\delta) = \frac{d + (c - v_{\text{tx}}) t_\delta}{c - v_{\text{rx}}} \tag{11}$$

$$t_\delta = \xi^{-1}(\xi) = \frac{c - v_{\text{rx}}}{c - v_{\text{tx}}} \left(\xi - \frac{d}{c - v_{\text{rx}}} \right). \tag{12}$$

Finally, defining the Doppler scaling factor $\sigma = (c - v_{\text{rx}})/(c - v_{\text{tx}})$ and $\tau_0 = d/(c - v_{\text{rx}})$, we obtain:

$$y(t) = \sigma \rho(\sigma(t - \tau_0)) x(\sigma(t - \tau_0)), \tag{13}$$

showing that the received signal is affected by Doppler time scaling and a Doppler-induced amplitude shift proportional to σ. The absolute value in (6) was neglected since $\sigma > 0$ for $|v_{\text{tx}}|$ and $|v_{\text{rx}}| \ll c$.

2.2 Multipath propagation

In general, a number L of paths will reach the receiver. Every path will feature a different Direction of Departure, identified by a unit norm vector $\mathbf{u}_l^{\text{DoD}}$, from the transmitter and Direction of Arrival, identified by a unit norm vector $\mathbf{u}_l^{\text{DoA}}$, at the receiver.

Assuming that the transmitter and receiver move with velocity vectors respectively given by $\mathbf{v}_{\text{tx}}$ and $\mathbf{v}_{\text{rx}}$, the path-dependent Doppler scaling factor will result

$$\sigma_l = \frac{c - \mathbf{v}_{\text{rx}}^T \mathbf{u}_l^{\text{DoA}}}{c - \mathbf{v}_{\text{tx}}^T \mathbf{u}_l^{\text{DoD}}} \tag{14}$$

while the path delays $\tau_{l,0}$ will result altered, with respect to those computed for static nodes τ_l, by the factor

$$\tau_{l,0} = \tau_l \frac{c}{c - \mathbf{v}_{\text{rx}}^T \mathbf{u}_l^{\text{DoA}}} \tag{15}$$

Finally, the received signal model for a noiseless linear time-varying multipath channel will result

$$y(t) = \sum_{l=1}^{L} \sigma_l \rho_l(\sigma_l(t - \tau_{l,0})) x(\sigma_l(t - \tau_{l,0})). \tag{16}$$

2.3 Complex envelope of a passband signal

Underwater Acoustic Communication systems operate in definite bands, and treating the transmitted and received signals as passband is attractive from the point of view of receiver complexity, as the baseband processing sampling rate may be reduced to only accommodate the bandwidth of the complex envelope.

We consider a passband transmitted signal obtained as

$$x(t) = \Re \left\{ \underline{x}(t) e^{j2\pi f_c t} \right\} \tag{17}$$

where $\underline{x}(t)$ is the complex envelope of the transmitted signal, and f_c is the carrier frequency with respect to which the complex envelope is extracted (usually the center of the band).

Substituting the transmitted signal expression into (16), we obtain the following expression for the complex envelope of the channel output:

$$\underline{y}(t) = \sum_{l=1}^{L} \tilde{\rho}_l \underline{x}(\sigma_l(t - \tau_{l,0})) e^{j2\pi f_c(\sigma_l - 1)t} \tag{18}$$

where $\tilde{\rho}_l \approx \sigma_l \rho_l(\sigma_l(t - \tau_{l,0})) e^{-j2\pi f_c \sigma_l \tau_{l,0}}$ is assumed to be approximately constant during one transmission burst.

It is necessary to note that a path-dependent Doppler scaling results in a combination of scaled and frequency shifted replicas of the transmitted signal, where a scaling factor of σ_l is paired with a Doppler-induced frequency shift equal to $f_c(\sigma_l - 1)$. With RF transmissions, the Doppler scaling effect is usually neglected as (at most) comparable to quartz crystal oscillator timing drifts, and the frequency shift term is the only readily observable Doppler phenomenon. Conversely, in the UWAC scenario, even relatively low transmitter and receiver velocities on the order of meters per

second, result in large scaling errors that would only be obtained for exceedingly high relative velocities in the RF scenario.

Also note that, in the context of RF communications, the Doppler spread quantifies the bandwidth over which a sinusoidal tone is spread, and this quantity is approximately constant over the bandwidth of the signal (a.k.a. the *narrowband* hypothesis). For UWAC, the Doppler spread should not be defined as a (frequency-dependent) frequency span, but instead as a range of covered scaling factors (*wideband*). Unless the scaling factor is the same for all paths, or there is a dominant path such that the contributions of other scaling factors result negligible, an intuitive definition of channel frequency response seems unfeasible.

3 Channel Estimation

By channel estimation we mean estimation of delays, amplitudes, and Doppler scaling factors of every path received with sufficient strength.

The reason for channel estimation is that knowledge of these parameters is useful to adapt the transmitted signal for the best performance, eventually choosing the most suitable modulation format for the scenario and/or adapting the modulation parameters for the best trade-off between reliability and spectral efficiency [23]. It is also necessary in order to use complex receiver structures that hypothesize knowledge of the channel parameters, such as [18].

Accurate channel estimation also allows advanced sensing on multi-transducer nodes, enabling accurate Direction of Arrival estimation and providing essential information for effective beamforming, in turn useful to reduce the effective Doppler spread and enable highly spectral efficient modulation formats, with low-complexity receiver structures, in otherwise unfeasible scenarios.

3.1 Maximum Likelihood channel estimation

The channel estimation problem for passband channels could be solved by suitable design of a training sequence $\underline{p}(t) \in \mathbb{C}$ of duration T_p, whose ambiguity function results *well localized* in the delay-scale domain

$$A_p(\tau,\sigma) = \int \underline{p}^*(t)\underline{p}(\sigma(t-\tau))e^{j2\pi f_c(\sigma-1)t}dt \tag{19}$$

that is, $|A_p(\tau,\sigma)|$ features a sharp maximum in both the delay and scale domains [5].

The transmitter would then transmit $\underline{p}(t)$ by upconversion (17), and the receiver would feature a bank of correlators (or equivalent basis projection) with a set of predefined scaling factors, obtaining a noisy sampled version of a linear combination of $A_p(\tau,\sigma)$. Each peak in the delay-scale domain would correspond to a different path and scaling factor, and the amplitude estimation would be carried out by linear projection on the signal basis corresponding to the set of identified delays and scales.

The described method would require a computational complexity proportional to the product between the number of samples used to represent the scaled and frequency shifted versions of $\underline{p}(t)$, and the number of predefined scaling factors. It is usually implemented as Orthogonal Matching Pursuit or a variation aimed at reducing its computational complexity [3, 6, 15]. It is necessary to note that the delay-domain resolution is limited (Heisenberg's principle) by the bandwidth of the signal $\underline{p}(t)$, and the scale-domain resolving power results directly proportional to the duration of the sequence itself.

Another factor that cannot be neglected is that the UWAC environment cannot be considered static, so the duration T_p of the training sequence is the result of a trade-off between the energy of the sequence and the per-path coherence time, i.e. the duration over which a path in a multipath channel can be considered affected by the same scaling factor.

In this paper, we are interested in low-complexity channel estimation approaches and will not further consider the correlation bank solution, nor a possibly equivalent Wavelet Transform-based method [22].

3.2 Sparse delay channels

A low-complexity solution to the Doppler scale estimation problem is readily obtained in the case of sparse delay channels, that is channels for which the minimum distance between consecutive arrivals is longer than the duration of a transmission burst. This is the case, for example, of UWAC scenarios where the propagation doesn't result in multiple paths with comparable delays, and the transmitter and receiver depths are such that paths reflected from the bottom and/or the top interfaces experience a large delay increase. This usually requires both the transmitter and receiver to be far from acoustic impedance interfaces (deep sea).

In this case, it can be assumed that the received replicas will be received independent of each other, and each one will feature its own Doppler scaling factor [4, 7–9, 11, 17, 19–21].

A low-complexity Doppler scale estimation method in this case may exploit a suitably introduced periodicity in the transmitted signal. One possibility would be to use a sounding signal $\underline{p}(t)$ of duration T_p, and transmitting two copies of $\underline{p}(t)$ delayed T_0 from each other [17]. Note that a similar effect is obtained by transmitting the desired modulated signal with a cyclic prefix, where the time distance between the cyclic prefix and its repetition within the signal is T_0 [9, 19].

The receiver may then obtain an estimate of the delay and Doppler scale by looking for maxima in the autocorrelation of the received signal, within intervals where the normalized autocorrelation is above a detection threshold. Setting the detection threshold depends on the desired false positive (or, depending on the application, false negative) probability.

The normalized autocorrelation allows the receiver to detect periodic features in the incoming signal, while the plain autocorrelation allows to estimate the delay. Since the periodicity T_0 is altered by the Doppler scaling, the receiver will need to compute the normalized autocorrelation over a period T_p/σ with delay T_0/σ, for a predefined set of σ values:

$$\gamma_y(\tau,\sigma) = \frac{\int_0^{T_p/\sigma} \underline{y}^*(t+\tau)\underline{y}(t+\tau+T_0/\sigma)dt}{\sqrt{\int_0^{T_p/\sigma}|\underline{y}(t+\tau)|^2dt\int_0^{T_p/\sigma}|\underline{y}(t+\tau+T_0/\sigma)|^2dt}}. \tag{20}$$

This search may be conducted with low complexity by sensible choice of the scaling factors σ, i.e. such that the delays T_0/σ result equal to an integer number of samples. In this case, denoting with T_s the sampling interval, with $D = T_0/\sigma T_s$ the integer delay and with $M = \lfloor T_p/\sigma T_s \rfloor$ the correlation interval, the receiver will

need to compute moving averages over M points of the sequences $\underline{y}^*(n)\underline{y}(n+D)$, $|\underline{y}(n)|^2$ and $|\underline{y}(n+D)|^2$, each of which requires only one complex multiplication, and a memory buffer of length D will be necessary to avoid repeated computations.

The overall multiplication complexity of computing this set of moving averages and the ratios (20) will be equal to four times the number of tested scaling factors, for every incoming sample. This results lower than the complexity of computing the output of the bank of correlators described in section 3.1, when the order of the filters M, corresponding to the duration of the signal $\underline{p}(t)$, is longer than four samples. That would be *always*, recalling that the duration of $\underline{p}(t)$ will need to be much longer for direct Doppler scale estimation.

While this method features a low complexity Doppler scale estimation (and signal presence detection), it catastrophically fails when the sparse delays hypothesis is not met. In fact, when the received signal results in a superposition of replicas affected by different Doppler scaling factors, the periodicity test (20) will fail, and no estimate will be obtained. The sparse delays hypothesis will not be met for shallow water scenarios, where the paths interacting with the interfaces will feature slightly differing delays with highly diverse angles of departure and arrival, resulting in a large Doppler scale spread.

4 Hyperbolic chirps

The impossibility of relying on a simple periodicity test such as (20) requires a low-complexity method for Doppler scale estimation and signal presence detection.

An Hyperbolic chirp (HC) [1] is designed to maintain its properties even after a scale change: it is defined as a constant envelope frequency modulated signal (in short, *chirp*) with instantaneous frequency given by:

$$f_i(t) = \frac{1}{\frac{1}{f_1} + \left(\frac{1}{f_2} - \frac{1}{f_1}\right)\frac{t}{T_p}}. \tag{21}$$

The analytic expression for an hyperbolic chirp is

$$p(t) = \Re\left\{e^{-\jmath\frac{2\pi}{\mu}\log(1-\mu f_1 t)}\right\} \tag{22}$$

where $\mu = \frac{f_2 - f_1}{f_1 f_2 T_p}$ is the chirp rate parameter, and f_1 and f_2 are the instantaneous frequencies for $t = 0$ and $t = T_p$ respectively. Note that this is not the complex envelope of the hyperbolic chirp, but the baseband expression.

The hyperbolic trend in instantaneous frequency results in a linearly varying *period*, which is the feature that makes hyperbolic chirps resilient to Doppler scaling.

In detail, after Doppler scaling with a factor σ, the resulting instantaneous frequency is given by

$$f_i^R(t) = \sigma f_i(\sigma t) \tag{23}$$

Setting a target instantaneous frequency f_T, a delayed and Doppler-scaled hyperbolic chirp instantaneous frequency will equate f_T at a time $t_{f_T}(\tau, \sigma)$ given by

$$t_{f_T}(\tau, \sigma) = \tau + \frac{T_p}{\sigma}\frac{\frac{1}{f_1} - \frac{\sigma}{f_T}}{\frac{1}{f_1} - \frac{1}{f_2}}. \tag{24}$$

The Doppler-invariant property of HCs is proven by checking that $t_{f_2}(\tau, \sigma) - t_{f_1}(\tau, \sigma) = T_p$ for any τ and σ. Note that a scaled HC will not cover the whole range $[f_1, f_2]$ but instead the range $[\sigma f_1, \sigma f_2]$.

Also note that (24) shows that Doppler scaling a HC results in an apparent delay (or advance) of the received signal, i.e. the scale-invariance property results in a delay estimation ambiguity.

4.1 Detection of a hyperbolic chirp

Let us assume that the transmitter operates in a band between f_L and f_H, low and high frequency bounds respectively. If the channel is affected by a unknown Doppler scaling upper bounded by a $\sigma_{\max} = (c + v_{\max})/(c - v_{\max})$, with $v_{\max}$ the maximum expected transmitter or receiver velocity, the receiver will need to observe the frequency range $[f_L/\sigma_{\max}, f_H\sigma_{\max}]$.

So, if the duration of the transmitted HC is T_p, the receiver will need to correlate with an extended HC with the expected chirp rate μ, and duration equal to

$$T_p^R = T_p \frac{\frac{1}{f_L/\sigma_{max}} - \frac{1}{f_H\sigma_{\max}}}{\frac{1}{f_L} - \frac{1}{f_H}}. \tag{25}$$

This precaution will allow the receiver to capture the whole energy of the received signals, regardless of the scaling factor. A test for normalized correlation above a detection threshold will allow the receiver to detect the presence of an incoming signal.

From a computational complexity point of view, the correlation can be performed with an FFT-based method, resulting in a complexity comparable to the bank of autocorrelators in the delay-sparse channel case.

4.2 Channel estimation with hyperbolic chirps

Due to the delay-scale ambiguity (24), a single HC cannot be used directly for delay and Doppler scale estimation.

Several papers, e.g. [8, 20], propose the joint use of up- ($\mu > 0$) and down- ($\mu < 0$) chirps, where for an upchirp $f_1 = f_L$, $f_2 = f_H$ and for a downchirp $f_1 = f_H$, $f_2 = f_L$. The idea is that, while both chirps will maintain their feature after scaling, the apparent delays (or advances) will appear in opposite directions for up- and down-chirps.

Two variations have been proposed: consecutive (with a known delay) up- and down- hyperbolic chirps, and superposed ones. The first option has the advantage of constant envelope and low peak-to-average power ratio (PAPR), which is a friendly option from the point of view of required power amplifier linearity and transducer efficiency. The second option has a slightly higher PAPR compensated by the advantage of simultaneous measurement, so that no assumption is needed on path coherence time.

When correlating a delayed and scaled upchirp $p(\sigma(t-\tau))$ with an (extended) hyperbolic upchirp at the receiver, a correlation peak will appear at a time t_U

$$t_U = \tau + \frac{T_p}{\sigma}\frac{\frac{1}{f_L} - \frac{\sigma}{f_L}}{\frac{1}{f_L} - \frac{1}{f_H}} \tag{26}$$

this expression was obtained by substituting $f_1 = f_L$, $f_2 = f_H$ and $f_T = f_L$ (the starting frequency) in (24).

Similarly, the correlation peak for a delayed and scaled downchirp will appear at:

$$t_D = \tau + \frac{T_p}{\sigma}\frac{\frac{\sigma}{f_H} - \frac{1}{f_H}}{\frac{1}{f_L} - \frac{1}{f_H}}. \tag{27}$$

To obtain a general result, useful both in the case of simultaneous and offset hyperbolic chirps, we assume that up- and down-chirps are transmitted with a known time offset T_{UD}. In this case, considering that the time offset T_{UD} gets scaled too, the measurable difference $t_U - t_D$ results equal to:

$$T^R_{\text{UD}} = t_U - t_D = \frac{T_{\text{UD}}}{\sigma} + \kappa\left(\frac{1}{\sigma} - 1\right), \tag{28}$$

where $\kappa = T_p\frac{f_L+f_H}{f_H-f_L}$, from which the estimate for the Doppler scaling factor σ is readily obtained:

$$\hat{\sigma} = \left(1 + \frac{\Delta\tau}{T_{\text{UD}} + \kappa}\right)^{-1} \tag{29}$$

where $\Delta\tau = T^R_{\text{UD}} - T_{\text{UD}}$ is the measured time offset, after removal of the known transmitted time offset.

When the offset $T_{\text{UD}} = 0$, the formula simplifies to [8, 20]

$$\hat{\sigma} = \frac{1}{1 + \Delta\tau/\kappa}. \tag{30}$$

Note that, in this latter case, the up- and down- chirps are transmitted simultaneously, so that it is necessary to assume that they result quasi-orthogonal and do not interfere significantly in the estimation of t_U and t_D.

An estimate for the delay τ is obtained indirectly from (26) and (27) as follows:

$$\hat{\tau} = \frac{t_U + t_D}{2} + \frac{T_p(\hat{\sigma} - 1) - T_{\text{UD}}}{2\hat{\sigma}} \tag{31}$$

Finally, path amplitude estimation is a linear estimation problem, and it is readily carried out by normalizing the amplitude of the correlation peak. Indeed, projection of the received signal (13) over $p(\hat{\sigma}(t - \hat{\tau}))$ corresponds, in the ideal estimation case, to

$$\int y(t)p(\sigma(t-\tau))dt = \tilde{\rho}\sigma\int |p(\sigma(t-\tau))|^2 dt = \tilde{\rho}\mathcal{E}_p \tag{32}$$

where $\tilde{\rho}$ is, by the mean value theorem, an approximation of $\rho(\sigma(t-\tau))$ within the duration T_p, and $\mathcal{E}_p$ is the energy of the hyperbolic chirp $p(t)$, approximately equal to $T_p/2$ if no windowing is used. Note that both the upchirp and the downchirp can be used for the amplitude estimation, and taking the average improves the estimate in the zero-mean noise case. Also note that the precaution of using an extended hyperbolic chirp at the receiver avoids windowing effects, so that the amplitude estimate results unaffected by the Doppler scale.

5 The time aliasing issue

Up to this point, we assumed that a single propagation path is present, with no real advantage of the hyperbolic chirp-based method with respect to the autocorrelation bank method, apart from an enhanced estimation accuracy that will be shown in the experimental evaluation.

We want to point out a problem that specifically affects channels affected by path-dependant Doppler scaling, that is time aliasing. Consider two paths, featuring respectively delays τ_i and τ_j, Doppler scales σ_i and σ_j and amplitudes ρ_i and ρ_j. The received signal will include the two contributions:

$$y_i(t) = \rho_i x(\sigma_i(t - \tau_i)) \tag{33}$$

$$y_j(t) = \rho_j x(\sigma_j(t - \tau_j)) \tag{34}$$

Consider a signal $x(t)$ transmitted starting from t_0. The received signal $y_i(t)$ will start from $t_{0,i} = \tau_i + t_0/\sigma_i$, while $y_j(t)$ will start from $t_{0,j} = \tau_j + t_0/\sigma_j$. For some combination of the parameters, the two times $t_{0,i}$ and $t_{0,j}$ can (and sometimes will) coincide.

This is especially an issue with hyperbolic chirps, as the chirp rate is invariant to changes in scale, so that if two received hyperbolic chirps interfere, they will interfere for their whole duration, leading to possibly severe fading and impairing the channel estimation effort. Also, this problem is more severe in the shallow water scenario, rich in multipath, with highly diverse Doppler scales.

5.1 Channel estimation for path-dependent Doppler

Following the argument used to show how time-aliasing can happen, it should be clear that the time-aliasing issue is time-selective, i.e. if two paths interfere at t_0, they will not interfere at earlier or later times.

For this reason, to solve the time-aliasing issue, we propose to use $N_{\text{pr}} \geq 2$ copies of the channel estimation preamble on doubly-spread channels. Although this is similar to the autocorrelation bank approach, it should be clear that the purpose of repeated transmissions is to have a chance to recover from time-aliasing issues, and no periodicity is expected in the received signal.

The receiver will compute the plain and normalized correlation with up- and down- hyperbolic chirps, and extract sets of (t_U, ρ_U) and (t_D, ρ_D) estimates. The estimates will be collected within intervals, starting from when a normalized correlation results above a detection threshold, and for a duration depending on the considered scenario.

The collected estimates $\{t_{U,1}, t_{U,2}, \dots\}$ from up-chirp correlations will need to be matched with the corresponding estimates $\{t_{D,1}, t_{D,2}, \dots\}$ from the down-chirp correlations. To this purpose, we use a greedy approach and match a correlation peak $t_{U,i}$ with a correlation peak $t_{D,j}$ if, and only if, $t_{D,j}$ is the only possible match for $t_{U,i}$, given the maximum Doppler scale $\sigma_{\max}$. Specifically, if a correlation peak is detected at $t_{U,i}$, the time interval within which a down-chirp correlation event is expected is:

$$t_{D,j} \in t_{U,i} + \kappa - (T_{\text{UD}} + \kappa)\left[\sigma_{\max}, \frac{1}{\sigma_{\max}}\right] \tag{35}$$

If no correspondence is found, or more than one $t_{D,j}$ falls within the interval, the correlation peak $t_{U,i}$ is skipped and the test is carried out for another $t_{U,i}$. After looping over every detected $t_{U,i}$, matching continues with the downchirp correlation instants, where an event $t_{D,j}$ is matched to $t_{U,i}$ if it is the only one within the interval

$$t_{U,i} \in t_{D,j} - \kappa + (T_{\text{UD}} + \kappa)\left[\frac{1}{\sigma_{\max}}, \sigma_{\max}\right]. \tag{36}$$

When two correlation positions t_U and t_D are matched, we can use (29) and (31) to estimate σ and τ. Since more than a preamble

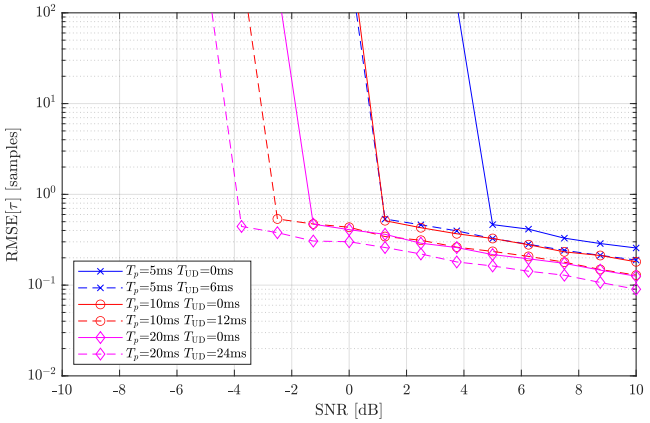

Figure 1: Root Mean Squared Error for τ estimates (samples) vs Signal-to-Noise Ratio, for $T_p = \{5, 10, 20\}$ms and $T_{UD} = \{0, 1.2T_p\}$

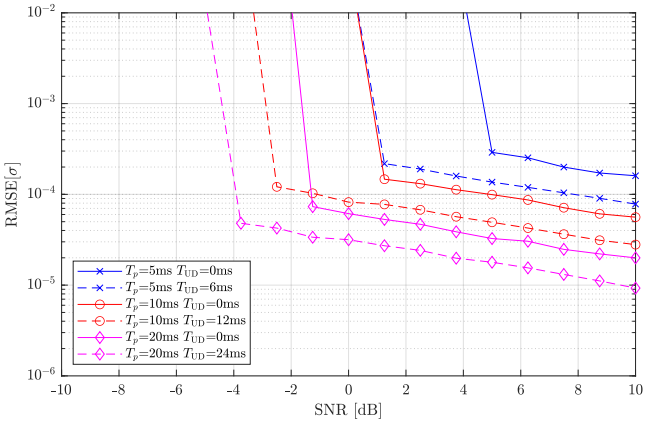

Figure 2: Root Mean Squared Error for σ estimates vs Signal-to-Noise Ratio, for $T_p = \{5, 10, 20\}$ms and $T_{UD} = \{0, 1.2T_p\}$

is transmitted, with a known delay T_0, we can then check if the corresponding correlation events after a delay T_0/σ were found and mark those as used. The matching continues until no further correlation events can be matched.

Note that this algorithm may miss some paths if time-aliasing occurs in every repetition of the preamble, so that experimental evaluation is needed in order to assess its performance.

6 Performance evaluation

We first evaluate the performance of the joint delay and Doppler scale estimation method for a single path channel, affected by constant Doppler scaling, for varying signal-to-noise ratio and preamble configuration.

Then we proceed with analysis of the proposed method for multipath scenarios, describing how the simulations were conducted, and showing how the preamble repetition is able to mitigate the time aliasing phenomenon we described.

Finally, we present a quantitative example of computational complexity of the proposed method, compared to the autocorrelation bank method and orthogonal matching pursuit.

6.1 Single path evaluation

Figures 1 and 2 show the root mean squared errors for τ and σ estimates, with Doppler scales covering the full range $\sigma \in [0.98, 1/0.98]$ and a sampling frequency of $f_s = 192$kHz, $f_L = 18$kHz, $f_H = 34$kHz. Three choices for $T_p = \{5, 10, 20\}$ms and $T_{UD} = 0$ (overlapping hyperbolic chirps) or $T_{UD} = 1.2T_p$ (consecutive hyperbolic chirps) were considered. The signal-to-noise ratio was evaluated as the ratio between the power of the preamble, that is $P_s = 1$ for $T_{UD} = 0$ and $P_s = 1/2$ for $T_{UD} = 1.2T_p$, and the receiver input noise $P_n = (f_H - f_L)N_0$, with the assumption of Additive White Gaussian Noise (AWGN).

For single-path evaluation, we chose to use $T_{UD} = 1.2T_p$ in order to avoid interference between the extended hyperbolic chirps used at the receiver for the correlations and the received signals. As expected, opting for an offset between the up- and down- hyperbolic chirps results in a gain of approximately 3dB. Longer training symbols appear to show diminishing gains in our setup. Conversely, shorter training symbols result in higher asymptotic RMSEs (without showing error floors).

The RMSE for σ estimates is always lower than $3 \cdot 10^{-4}$, resulting in an accurate velocity estimate, below 0.2m/s in the case of a static receiver. The RMSE for τ estimates is always below the sampling interval, thanks to the parabolic interpolation method [10] that can always be used when the sampling rate is at least four times the signal bandwidth. As it is apparent from both figures, the main difference between the various configurations is the SNR detection threshold. For the following evaluation, we choose to use $T_{UD} = 0$.

6.2 Multipath evaluation

For performance evaluation in multipath scenarios we performed MATLAB-based simulations, using the BellHop ray-tracer [16] to determine the static delays, amplitudes and angles of departure and arrival for every path. For every simulation run, we randomly generated the velocity and direction of the transmitter and receiver, computed the Doppler scale factors according to the ray-traced angle of departure and arrival, and delayed and scaled the transmitted sequences. We did add a small amount of AWGN noise, so the signal-to-noise ratio resulted very high, exceeding 100dB. The reason to consider such a high signal-to-noise ratio is that we want to evaluate the intrinsic capability of the method to detect even the faintest path.

We considered a sparse delay case, corresponding to the Kauai example from the BellHop User Manual [13], and several shallow water cases obtained simply reducing the sea bottom depth.

Table 1 reports the parameters needed to reproduce the considered scenarios, i.e. transmitter and receiver depth, horizontal distance and sea bottom depth. Table 2 reports RMS delay spread, maximum delay and Doppler scale spread of every scenario, for random TX and RX direction and velocities up to 15m/s. The RMS delay spread and Doppler spread have been obtained weighting each contribution with $|\rho_l|^2 / \sum |\rho|^2$ [10].

Scenario	depth (m)	TX depth (m)	RX depth (m)
Kauai	971	323	485
K600	600	280	300
K200	200	86	100
K60	60	20	30
K20	20	6	10

Table 1: Geometric configuration of the considered scenarios. The horizontal distance is 500 meters.

Scenario	RMS d.s.(ms)	$\max\tau - \min\tau$ (ms)	Doppler spr.
Kauai	152.7	1500	$2.5 \cdot 10^{-3}$
K600	127.3	1300	$2.47 \cdot 10^{-3}$
K200	26.78	880	$1.15 \cdot 10^{-3}$
K60	8.04	150	$9.38 \cdot 10^{-4}$
K20	2.56	31	$6.13 \cdot 10^{-4}$

Table 2: Spread parameters of the considered scenarios. The Doppler spread is the standard deviation of the scaling factor.

Scenario	Pr{det.}	RMSE[σ]	RMSE[τ/T_s]	RMSE[ρ] %
Kauai	100%	$1.26 \cdot 10^{-7}$	$3.42 \cdot 10^{-4}$	$5.02 \cdot 10^{-4}$
K600	100%	$1.44 \cdot 10^{-7}$	$3.38 \cdot 10^{-4}$	$6.66 \cdot 10^{-4}$
K200	100%	$5.75 \cdot 10^{-5}$	$1.54 \cdot 10^{-1}$	1.26
K60	70.5%	$1.13 \cdot 10^{-4}$	0.287	4.4
K20	0%	NaN	NaN	NaN

Table 3: Results for noiseless scenarios with maximum receiver and transmitter velocity 15m/s, preamble duration 10ms, one repetition.

Table 3 shows the probability of path detection Pr{det.} and root mean squared errors obtained in the described scenarios, for a high signal-to-noise ratio (exceeding 100dB), for a preamble duration T_p = 10ms. Note that the Kauai and K600 scenarios have a minimum separation between consecutive delays of 206ms and 24ms respectively, so fall in the sparse delay scenario. The K200 scenario has a minimum delay separation of 8.8ms, and the channel estimation almost always succeeded in detecting every path and accurately extract the delay, Doppler and amplitude parameters.

The K60 scenario has a minimum delay separation of 1.45ms, but thanks to the relatively large delay spread it is still possible to detect almost every path, while the RMSE for the parameters degrade considerably. In the K20 scenario, the minimum separation between paths is 0.17ms and the RMS delay spread is only 2.56ms, so the method fails most of the time, detecting on average only 23% of the received paths.

In order to improve the channel estimation performance of the method in the shallow water scenarios, we evaluated the effect of reducing the duration of the preamble and exploit the repeated transmission method.

The figures 3 and 4 show the probability of path detection, and the corresponding RMSE of σ estimates, versus the preamble duration T_p in the considered scenarios. The scenarios Kauai, K600 and K200 have a 100% probability of detection for every duration

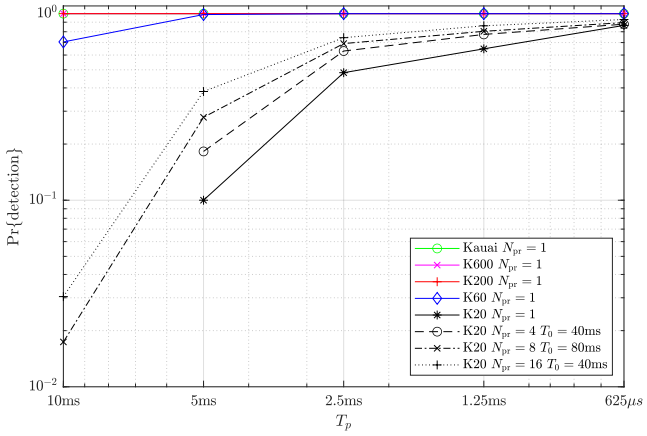

Figure 3: Probability of path detection versus preamble duration T_p, for the considered scenarios.

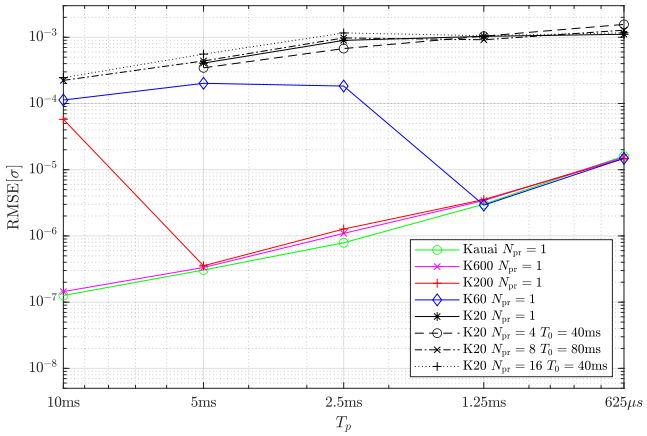

Figure 4: Root Mean Squared Error for σ estimates versus preamble duration T_p, for the considered scenarios.

between 625μs and 10ms, but the RMSE[σ] is not as low as expected from the single-path analysis when $T_p > 5$ms for K200. This can be explained as interference arising between the received preambles, since the minimum path separation for K200 is 8.8ms. In the same way, in the K60 scenario the probability of path detection is lower than 100% for T_p = 10ms and the RMSE[σ] diagram shows interference phenomena when $T_p > 1.25$ms (the minimum delay separation for K60 is 1.45ms).

The K20 scenario is the one for which the repeated preamble transmission method is both necessary and effective to improve the path detection probability. Indeed, the RMSE[σ] is approximately invariant to the number of repetitions N_{pr} and repetition delay T_0, while the probability of path detection is improved significantly. Also note that, in order to limit the self-interference between the received preambles, it is necessary to use preamble deurations shorter than 10ms. In our evaluation, we found that $T_p \leq 2.5$ms works well, with a probability of path detection higher than 75%, for $N_{\text{pr}} = 16$ and $D = 40$ms or similar overall duration combinations.

6.3 Quantitative complexity analysis

The proposed method requires post-processing the output of two correlators with the up- and down- extended hyperbolic chirps. These can be implemented with FFT-based methods and, depending of the sampling rate and operating bandwidth, can also be implemented processing the complex envelope.

To provide some quantitative analysis, we consider a receiver operating with f_s = 192kHz, f_L = 18kHz, f_H = 34kHz, and T_p = 10ms for the sparse-delay scenario, or $T_p = 625\mu$s, with T_0 = 40ms and $N_{\text{pr}} = 16$ for the doubly-spread scenario. In both scenarios we consider a $\sigma_{\max} = 1.02$.

In the delay-sparse scenario, the proposed method requires computing two normalized correlations (sharing normalization) with $T_p^R f_s = 2044$ samples, which can be carried out with an FFT-based method with $N_{\text{FFT}} = 4096$ points. The computational complexity, in terms of complex multiplications per second, results approximately

$$f_s \frac{3(N_{\text{FFT}} \log_2 N_{\text{FFT}} + N_{\text{FFT}})}{N_{\text{FFT}} - 2044} \approx 15\text{Mmul/s} \tag{37}$$

that is approximately 80 multiplications/sample. With this computational budget, The autocorrelation bank method can afford to use 20 scaling factors, with a $\Delta\sigma \approx 0.002$ and a comparable RMSE$[\sigma]$, which is much higher than the 10^{-7} found in this scenario.

In the doubly-spread scenario, the proposed method requires computing correlations with extended chirps made of 128 samples, resulting in a computational complexity of approximately 8Mmul/s with $N_{\text{FFT}} = 4096$. OMP-based methods require projection on scaled versions of the reference signals, and result in a higher complexity as soon as more than three scaled versions are used. They also require knowledge of the dimensionality of the received signal, and that is not readily available in operational scenarios without some other means for channel estimation.

7 Conclusions and further work

We presented a novel, low complexity method for channel estimation of doubly spread channels, and discussed its performance in terms of mean squared errors and computational complexity. As the simulation results show encouraging performance, we believe this method outperforms most of the existing methods, and can find application in operational scenarios. We plan to run measurements campaigns, whose results will be subject of further work.

Acknowledgments

This work was supported by the European Union - Next Generation EU under the Italian National Recovery and Resilience Plan (NRRP), Mission 4, Component 2, Investment 1.3, CUP E63C22002070006, partnership on "Telecommunications of the Future" (PE00000001 - program "RESTART")

References

[1] R.A. Altes. 1990. RADAR/SONAR Acceleration Estimation with Linear-Period Modulated Waveforms. *IEEE Trans. Aerospace Electron. Systems* 26, 6 (1990), 914–924. doi:10.1109/7.62244

[2] P. Bello. 1963. Characterization of Randomly Time-Variant Linear Channels. *IEEE Transactions on Communications Systems* 11, 4 (1963), 360–393. doi:10.1109/TCOM.1963.1088793

[3] Christian R. Berger, Shengli Zhou, James C. Preisig, and Peter Willett. 2010. Sparse Channel Estimation for Multicarrier Underwater Acoustic Communication: From Subspace Methods to Compressed Sensing. *IEEE Transactions on Signal Processing* 58, 3 (2010), 1708–1721. doi:10.1109/TSP.2009.2038424

[4] T.H. Eggen, A.B. Baggeroer, and J.C. Preisig. 2000. Communication over Doppler Spread Channels. Part I: Channel and Receiver Presentation. *IEEE Journal of Oceanic Engineering* 25, 1 (2000), 62–71. doi:10.1109/48.820737

[5] David A. Hague and John R. Buck. 2017. The Generalized Sinusoidal Frequency-Modulated Waveform for Active Sonar. *IEEE Journal of Oceanic Engineering* 42, 1 (2017), 109–123. doi:10.1109/JOE.2016.2556500

[6] Nicolas F. Josso, Jun Jason Zhang, Antonia Papandreou-Suppappolat, Cornel Ioana, Jerome I. Mars, Cédric Gervaise, and Yann Stephan. 2009. On the Characterization of Time-Scale Underwater Acoustic Signals using Matching Pursuit Decomposition. In *OCEANS 2009*. 1–6. doi:10.23919/OCEANS.2009.5422228

[7] Baosheng Li, Shengli Zhou, Milica Stojanovic, Lee Freitag, and Peter Willett. 2008. Multicarrier Communication Over Underwater Acoustic Channels With Nonuniform Doppler Shifts. *IEEE Journal of Oceanic Engineering* 33, 2 (2008), 198–209. doi:10.1109/JOE.2008.920471

[8] Zhiqiang Ling, Lei Xie, and Huifang Chen. 2019. Joint Doppler Scale Estimation and Timing Synchronization in Underwater Acoustic Communications. In *2019 IEEE International Conference on Signal Processing, Communications and Computing (ICSPCC)*. 1–6. doi:10.1109/ICSPCC46631.2019.8960868

[9] Sean F. Mason, Christian R. Berger, Shengli Zhou, and Peter Willett. 2008. Detection, Synchronization, and Doppler Scale Estimation with Multicarrier Waveforms in Underwater Acoustic Communication. *IEEE Journal on Selected Areas in Communications* 26, 9 (2008), 1638–1649. doi:10.1109/JSAC.2008.081204

[10] Umberto Mengali and Aldo N. D'Andrea. 1997. *Synchronization Techniques for Digital Receivers*. Springer New York, NY. doi:10.1007/978-1-4899-1807-9

[11] Habib Mirhedayati Roudsari and Jean-François Bousquet. 2019. A Time-Varying Filter for Doppler Compensation Applied to Underwater Acoustic OFDM. *Sensors* 19, 1 (2019). doi:10.3390/s19010105

[12] Roberto Petroccia and Joao Alves. 2024. The JANUS Underwater Communications Standard: From Promulgation to Present. In *OCEANS 2024 - Singapore*. 1–9. doi:10.1109/OCEANS51537.2024.10682419

[13] Michael B. Porter. 2011. *The BELLHOP Manual and User's Guide: Preliminary Draft*. Technical Report. Heat, Light, and Sound Research, Inc., La Jolla, CA, USA. http://oalib.hlsresearch.com/Rays/HLS-2010-1.pdf Accessed: 20 August 2025.

[14] Parastoo Qarabaqi and Milica Stojanovic. 2013. Statistical Characterization and Computationally Efficient Modeling of a Class of Underwater Acoustic Communication Channels. *IEEE Journal of Oceanic Engineering* 38, 4 (2013), 701–717. doi:10.1109/JOE.2013.2278787

[15] Fengzhong Qu, Xingyang Nie, and Wen Xu. 2015. A Two-Stage Approach for the Estimation of Doubly Spread Acoustic Channels. *IEEE Journal of Oceanic Engineering* 40, 1 (2015), 131–143. doi:10.1109/JOE.2014.2307194

[16] HLS Research. [n. d.]. Ocean Acoustics Library – Acoustics Toolbox. http://oalib.hlsresearch.com/AcousticsToolbox/. Accessed: 2025-08-20.

[17] B.S. Sharif, J. Neasham, O.R. Hinton, and A.E. Adams. 2000. A Computationally Efficient Doppler Compensation System for Underwater Acoustic Communications. *IEEE Journal of Oceanic Engineering* 25, 1 (2000), 52–61. doi:10.1109/48.820736

[18] Kai Tu, Tolga M. Duman, Milica Stojanovic, and John G. Proakis. 2013. Multiple-Resampling Receiver Design for OFDM Over Doppler-Distorted Underwater Acoustic Channels. *IEEE Journal of Oceanic Engineering* 38, 2 (2013), 333–346. doi:10.1109/JOE.2012.2221812

[19] Lei Wan, Hanbo Jia, Feng Zhou, Muhammad Muzzammil, Tao Li, and Yi Huang. 2020. Fine Doppler Scale Estimations for an Underwater Acoustic CP-OFDM System. *Signal Processing* 170 (2020), 107439. doi:10.1016/j.sigpro.2019.107439

[20] Kaixing Wang, Shumin Chen, Chenzhan Liu, Yangxi Liu, and Yuanxin Xu. 2015. Doppler Estimation and Timing Synchronization of Underwater Acoustic Communication Based on Hyperbolic Frequency Modulation Signal. In *2015 IEEE 12th International Conference on Networking, Sensing and Control*. 75–80. doi:10.1109/ICNSC.2015.7116013

[21] Xiaowei Yu, Yiyin Wang, and Xinping Guan. 2018. Doppler Scale Estimation for Underwater Acoustic Communications Using Dual Zadoff-Chu Sequences. In *2018 IEEE International Conference on Signal Processing, Communications and Computing (ICSPCC)*. 1–5. doi:10.1109/ICSPCC.2018.8567772

[22] Xing Zhang, Kang Song, Chunguo Li, and Luxi Yang. 2018. A Novel Approach for the Estimation of Doubly Spread Acoustic Channels Based on Wavelet Transform. *Applied Sciences* 8, 1 (2018). doi:10.3390/app8010038

[23] Muhammad Yousuf Irfan Zia, Javier Poncela, and Pablo Otero. 2021. State-of-the-Art Underwater Acoustic Communication Modems: Classifications, Analyses and Design Challenges. *Wireless Personal Communications* 116 (2021). Issue 2. doi:10.1007/s11277-020-07431-x